

Nonlinear hypocentre determination in the 3-D Western Bohemia a priori velocity model

Václav Bucha & Luděk Klimeš

*Department of Geophysics, Faculty of Mathematics and Physics, Charles University in Prague, Ke Karlovu 3, 121 16 Praha 2, Czech Republic,
<http://sw3d.cz/staff/bucha.htm>, <http://sw3d.cz/staff/klimes.htm>*

Summary

The robust algorithm of nonlinear hypocentre determination is proposed. The algorithm has been coded in a flexible modular way for testing purposes. The method and application of the code is illustrated on a numerical example of hypocentre determination of four local earthquakes in the a priori 3-D velocity model of the seismically active part of Western Bohemia.

Keywords

Hypocentre determination, velocity model, accuracy of the velocity model, model covariance function, geometrical travel-time covariance matrix, marginal a posteriori density function of hypocentral coordinates, arrival-time residuals, arrival-time misfit.

1. Introduction

This paper demonstrates a flexible and robust method for nonlinear hypocenter determination. The method is based on direct evaluation of the nonnormalized 3-D marginal a posteriori density function which describes the relative probability of the seismic hypocentre (Tarantola & Valette, 1982). The method has been used with the first-arrival travel times by Moser, Van Eck & Nolet (1992), whereas we use it with the ray-theory travel times. The theory underlying the method is summarized by Bulant & Klimeš (2015).

The multivalued ray-theory travel times from the receivers to the gridpoints of a 3-D spatial grid of points can efficiently be calculated in the velocity model using the controlled initial-value ray tracing (Bulant, 1996; 1997; 1999; 2012) followed by the interpolation of travel times within ray cells (Bulant & Klimeš, 1999). The controlled initial-value ray tracing uses the initial-value ray tracing algorithm according to Červený, Klimeš & Pšenčík (1988).

In order to estimate the uncertainty of the hypocentral position, we also need to know the uncertainty of the measured arrival times and the uncertainty of the velocity model. The uncertainty of the measured arrival times is expressed in terms of the data covariance matrix of the measured arrival times, which is usually diagonal and composed of the squares of the standard deviations of the measured arrival times. The uncertainty of the velocity model is expressed in terms of the model covariance function (Franklin, 1970; Tarantola & Valette, 1982; Tarantola & Nercessian, 1984; Tarantola, 1987; Klimeš, 2002a) which is projected onto the uncertainty of the hypocentral position through the geometrical covariances of theoretical travel times calculated in the velocity model (Klimeš, 2002b; 2008). In order to estimate the uncertainty of the hypocentral

position, we thus need the standard deviations of the measured arrival times, and the geometrical covariances of theoretical travel times calculated using the model covariance function.

For the sake of simplicity and rapid numerical implementation, we consider just the diagonal elements of the geometrical travel–time covariance matrix in this paper. We are going to propose the numerical algorithm of calculating the whole geometrical travel–time covariance matrix at the gridpoints of a 3–D spatial grid in the near future.

In Section 2, we describe the numerical algorithm of nonlinear hypocentre determination, based on the equations by Bulant & Klimeš (2015). We concentrate on directly calculating the nonnormalized 3–D marginal a posteriori density function which describes the relative probability of the seismic hypocentre. The calculated nonnormalized 3–D marginal a posteriori density function is discretized at the gridpoints of a sufficiently dense 3–D spatial grid of points.

In Section 3, we test the first version of the computer code for nonlinear hypocentre determination using four examples of local earthquakes recorded on January 1997 by the WEBNET local seismic network.

2. Numerical algorithm

The nonlinear hypocentre determination is composed of two main steps. The first step consists in computing theoretical travel times in the 3–D velocity model at the nodes of a dense rectangular grid covering the region where the hypocentre is searched for.

In the second step, we use the theoretical travel times, their standard deviations, measured arrival times and their standard deviations for the determination of the nonnormalized 3–D marginal a posteriori density function which describes the relative probability of the seismic hypocentre.

2.1. Travel times on a spatial grid of points

The nature of the theoretical travel times should correspond to the measured travel times. For instance, first–arrival travel times calculated by an eikonal solver or multivalued ray–theory travel times corresponding to a specified elementary wave may be considered.

We consider the ray–theory travel times. For their computation, we use software packages FORMS, MODEL and CRT (Červený, Klimeš & Pšenčík, 1988; Bucha & Bulant, 2015).

A sufficiently dense system of rays for each considered elementary wave from each receiver is computed in the whole 3–D model by controlled initial–value ray tracing (Bulant, 1996; 1997; 1999; 2012). The travel times at the gridpoints of the 3–D location grid are then obtained by the interpolation of travel times within ray cells (Bulant & Klimeš, 1999).

2.2. Nonlinear hypocentre determination on a spatial grid of points

The numerical algorithm of hypocentre determination is based on the equations summarized by Bulant & Klimeš (2015, sec. 2).

Input data for the hypocentre determination algorithm consist in N arrival times T_i , $i = 1, 2, \dots, N$ with their standard deviations ΔT_i , and in theoretical travel times τ_i calculated in the velocity model and discretized at the nodes of a sufficiently dense 3-D grid of points. We assume that standard deviations $\Delta\tau_i$ of theoretical travel times read (Bulant & Klimeš, 2015, eq. 55)

$$\Delta\tau_i = \sigma \left(\frac{\tau_i}{\theta} \right)^{1+H}, \quad (1)$$

where H is the Hurst exponent, and σ is the travel-time standard deviation at reference travel time θ .

Similarly as Bulant & Klimeš (2015, sec. 6.1), we neglect all off-diagonal elements of the matrix of geometrical covariances of theoretical travel times although we know that it is incorrect.

At the nodes of the 3-D grid of points used for the hypocentre determination, we define three sums

$$a_n = \sum_{i=1}^n (\Delta\tau_i^2 + \Delta T_i^2)^{-1}, \quad (2)$$

$$b_n = \sum_{i=1}^n (\Delta\tau_i^2 + \Delta T_i^2)^{-1} (T_i - \tau_i) \quad (3)$$

and

$$d_n = \sum_{i=1}^n (\Delta\tau_i^2 + \Delta T_i^2)^{-1} (T_i - \tau_i)^2. \quad (4)$$

These sums can be accumulated receiver by receiver as

$$a_n = \sum_{i=1}^n \Delta a_n \quad (5)$$

with

$$\Delta a_n = (\Delta\tau_i^2 + \Delta T_i^2)^{-1}, \quad (6)$$

$$b_n = \sum_{i=1}^n \Delta b_n \quad (7)$$

with

$$\Delta b_n = \Delta a_n (T_i - \tau_i), \quad (8)$$

and

$$d_n = \sum_{i=1}^n \Delta d_n \quad (9)$$

with

$$\Delta d_n = \Delta b_n (T_i - \tau_i). \quad (10)$$

The discretized hypocentral time then reads (Bulant & Klimeš, 2015, eq. 14)

$$h = \frac{b_N}{a_N} \quad , \quad (11)$$

and its standard deviation is (Bulant & Klimeš, 2015, eq. 16)

$$\Delta h = (a_N)^{-\frac{1}{2}} \quad . \quad (12)$$

The nonnormalized 3-D marginal a posteriori density function which describes the relative probability of the seismic hypocentre reads (Bulant & Klimeš, 2015, eq. 17)

$$\sigma_{P3} = \exp \left(-\frac{1}{2} c_N \right) \quad , \quad (13)$$

where

$$c_N = d_N - \frac{b_N^2}{a_N} \quad . \quad (14)$$

Since the subtraction in relation (14) introduces rounding errors into the numerical algorithm, we do not calculate c_N using summation (9) and relation (14). Instead, we define

$$c_n = d_n - \frac{b_n^2}{a_n} \quad , \quad (15)$$

and calculate c_N directly using sums

$$c_n = \sum_{i=1}^n \Delta c_n \quad (16)$$

with positive increments Δc_n . Inserting sums (5), (7), (9) and (16) into definition (15), we obtain relation

$$\Delta c_n = \Delta d_n - \frac{(b_{n-1} + \Delta b_n)^2}{a_n} + \frac{(b_{n-1})^2}{a_{n-1}} \quad , \quad (17)$$

which we express as

$$\Delta c_n = \frac{\Delta d_n a_{n-1} (a_{n-1} + \Delta a_n) - (b_{n-1} + \Delta b_n)^2 a_{n-1} + (b_{n-1})^2 (a_{n-1} + \Delta a_n)}{a_{n-1} a_n} \quad . \quad (18)$$

Two squares in the numerator of expression (18) partially cancel,

$$\Delta c_n = \frac{\Delta d_n a_{n-1} (a_{n-1} + \Delta a_n) - 2b_{n-1} \Delta b_n a_{n-1} - (\Delta b_n)^2 a_{n-1} + (b_{n-1})^2 \Delta a_n}{a_{n-1} a_n} \quad . \quad (19)$$

We insert definitions (8) and (10) into expression (19), and obtain

$$\Delta c_n = \frac{(T_i - \tau_i)^2 a_{n-1}^2 \Delta a_n - 2b_{n-1} (T_i - \tau_i) \Delta a_n a_{n-1} + (b_{n-1})^2 \Delta a_n}{a_{n-1} a_n} \quad , \quad (20)$$

which reads

$$\Delta c_n = \frac{[(T_i - \tau_i) a_{n-1} - b_{n-1}]^2}{a_{n-1} a_n} \Delta a_n \quad . \quad (21)$$

Since the algorithm of nonlinear hypocentre determination consists in calculations at the nodes of a 3-D grid of points, the above proposed numerical algorithm has been coded in the form of command files `loc0.cal`, `loc1.cal` and `loc2.cal` for program `grdcal.for` which performs calculations at the nodes of a grid of points. Command

files `loc0.cal`, `loc1.cal` and `loc2.cal` are located in package FORMS (Bucha, Bulant & Klimeš, 2000).

Command file `loc0.cal` just initiates sums (5), (7) and (16) to zeros by writing grid values $a_0 = 0$, $b_0 = 0$ and $\sqrt{c_0} = 0$.

Command file `loc1.cal` is used for each measured arrival time corresponding to the event, and calculates sums (5), (7) and (16) composed of contributions (6), (8) and (21). Note that command file `loc1.cal` calculates c_n , but reads and writes $\sqrt{c_n}$ instead of c_n . Command file `loc1.cal` thus reads the grid values of a_{n-1} , b_{n-1} and $\sqrt{c_{n-1}}$. It then calculates and writes the grid values of a_n , b_n and $\sqrt{c_n}$.

Command file `loc2.cal` finally reads the grid values of sums a_N , b_N and $\sqrt{c_N}$, and converts them into discretized hypocentral time (11), its discretized standard deviation (12), and the nonnormalized 3-D marginal a posteriori density function (13) which describes the relative probability of the seismic hypocentre.

The value y of the *arrival-time misfit* can be obtained from the maximum σ_{P3}^{\max} of the nonnormalized marginal a posteriori density function $\sigma_{P3}(x_i)$ of hypocentral coordinates as (Bulant & Klimeš, 2015, eq. 29)

$$y = -2 \ln(\sigma_{P3}^{\max}) \quad . \quad (22)$$

3. Numerical example

The above mentioned code is tested here by determining hypocentres of four local earthquakes recorded on January 1997 by the WEBNET local seismic network and one receiver in Germany, see Figures 1 and 2. Three tested local earthquakes were measured by 10 receivers and one event was recorded by 6 receivers. Table 1 displays the coordinates of the receivers, and Table 2 contains arrival times of four local earthquakes. Errors of the determination of arrival times are 4 ms for all receivers, except TRC and VIEL with 8 ms (J. Horálek, Geophysical Institute, personal communication).

<i>receiver</i>	<i>X</i>	<i>Y</i>	<i>Z</i>
CAC–Částkov	1012.285	877.220	0.578
KOC–Kopaniny	999.990	894.369	0.582
KRC–Kraslice	996.160	872.307	0.754
LAC–Lazy	1028.072	870.656	0.838
NKC–Nový Kostel	1006.015	879.876	0.568
SBC–Seeberg	1015.130	893.324	0.502
SKC–Škalná	1011.952	887.139	0.457
TRC–Trojmezí	994.770	899.922	0.566
VIEL–Viel	1007.031	904.927	0.670
ZHC–Zelená Hora	1022.225	892.640	0.631

Table 1: Receiver coordinates X, Y, Z (Křovák system in km and the elevation in km).

As the velocity model, we use the Western Bohemia a priori model, which was described in detail by Klimeš (1995), who created it manually as the initial velocity model for the iterative inversion of travel times from refraction seismic measurements. Refer to Bulant (1996) for ray tracing in the Western Bohemia a priori model. Figure 1

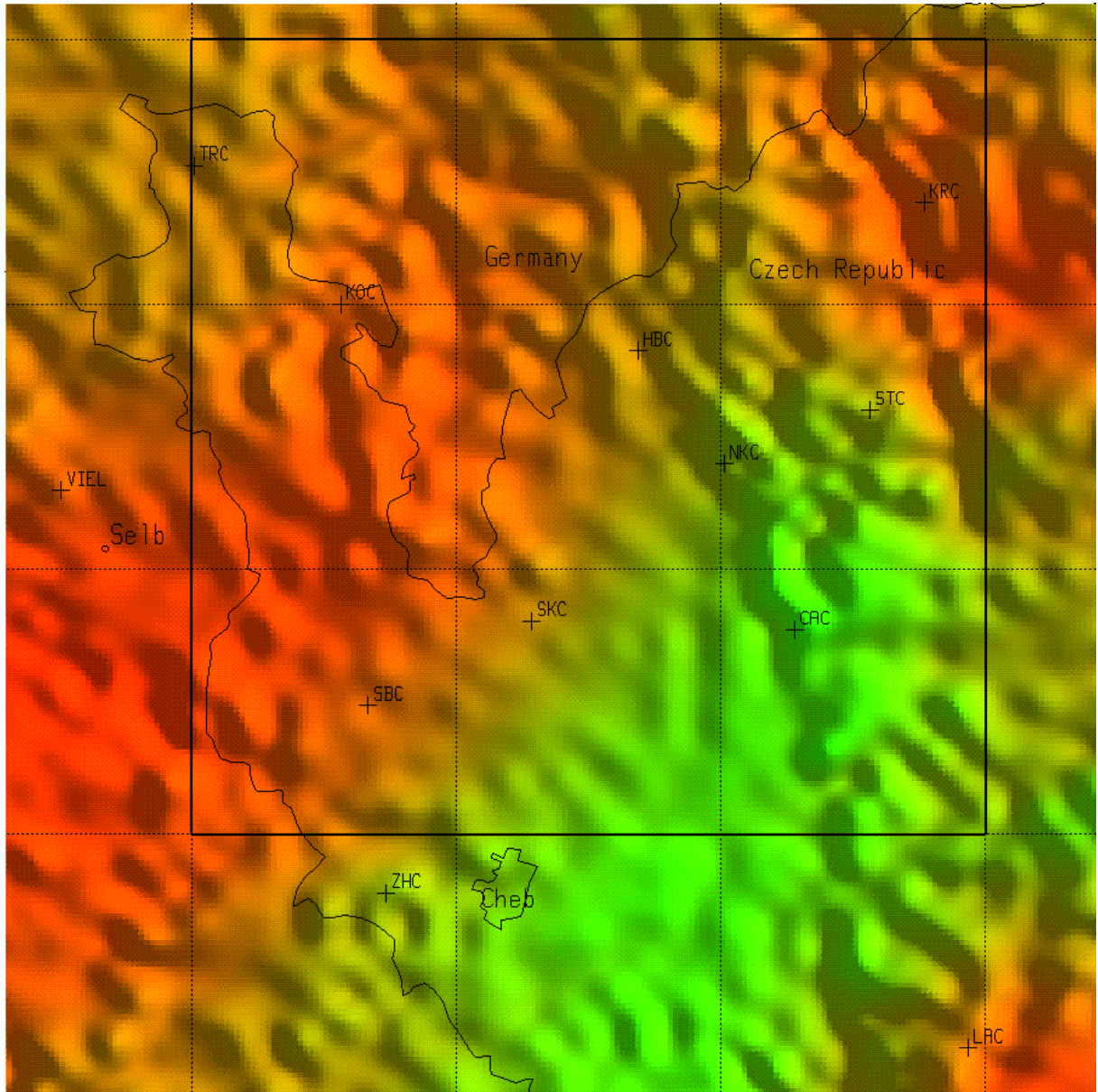


Figure 1: Part of the Western Bohemia a priori velocity model with the receivers and surface velocities (the shadows are caused by the topography). The thick line rectangle limits the location grid. Receivers HBC and STC are not considered.

displays a part of Western Bohemia a priori model with the surface P wave velocities (values of the velocity increase from green to red colour), and the positions of the receivers. The rectangle limits the location grid extending between the elevations of -17 km and 0 km. The dimensions of the grid are $\Delta X=30$ km, $\Delta Y=30$ km, $\Delta Z=17$ km. The grid step is 0.5 km in all three directions.

For the computation of ray-theory travel times in the 3-D Western Bohemia a priori velocity model, we use software packages FORMS, MODEL and CRT (Červený, Klimeš & Pšenčík, 1988; Bucha & Bulant, 2015). A sufficiently dense system of rays from each of 10 selected receivers is computed in the whole 3-D model by controlled initial-value ray tracing (Bulant, 1996; 1997; 1999; 2012). Only the P waves are considered. The travel times at the gridpoints of the 3-D location grid are then obtained by the

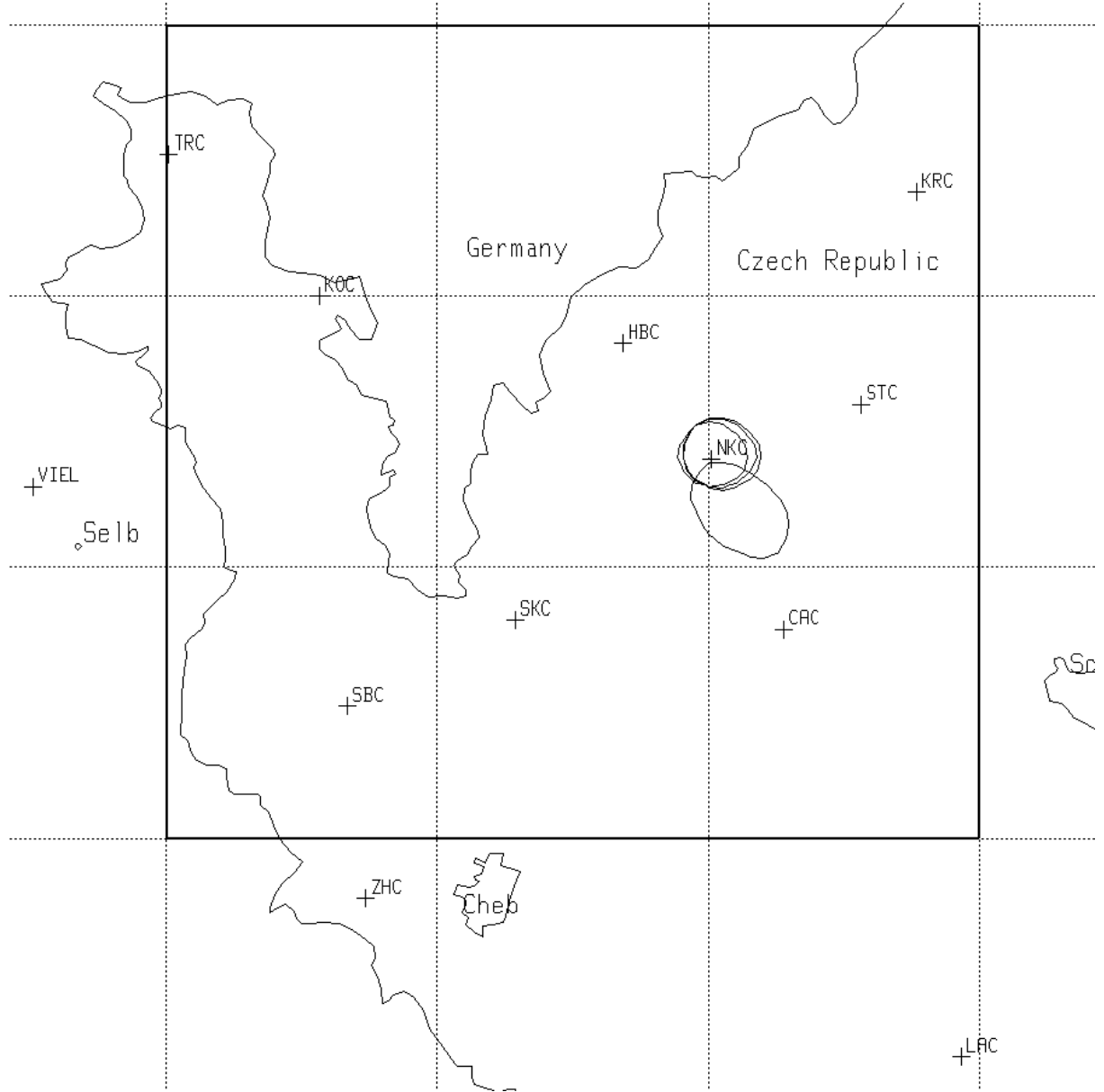


Figure 2: Seismically active region of Western Bohemia. The thick line rectangle limits the location grid. Four approximately elliptical curves limit the regions where the probability density functions of the four epicentres exceed 10% of the respective maximum values.

interpolation of travel times within ray cells (Bulant & Klimeš, 1999).

We do not know the accuracy of the 3-D Western Bohemia a priori velocity model. We thus substitute the correct standard deviations of theoretical travel times with the standard deviations corresponding to the 1-D mean model of the region by Klimeš (2002b, eq. 59). The standard travel-time deviations are given by relation (1) with deviation

$$\sigma = 0.062 \text{ s} \quad (23)$$

at reference travel time

$$\theta = 1 \text{ s} \quad , \quad (24)$$

and with Hurst exponent

$$H = -0.12 \quad (25)$$

<i>receiver</i>	<i>event 1</i>	<i>event 2</i>	<i>event 3</i>	<i>event 4</i>
CAC–Částkov	30.168	45.100	59.812	21.292
KOC–Kopaniny	31.316	46.228	60.972	22.788
KRC–Kraslice	30.856	45.804	60.484	22.292
LAC–Lazy	32.720	47.656	62.340	
NKC–Nový Kostel	29.856	44.748	59.512	21.060
SBC–Seeberg	31.472	46.372	61.108	22.672
SKC–Skalná	30.484	45.376	60.140	21.636
TRC–Trojmezí	32.432	47.352	62.072	
VIEL–Viel	32.672	47.584	62.312	
ZHC–Zelená Hora	32.132	47.036	61.768	

Table 2: Arrival times in seconds of four local earthquakes (P waves).

(Klimeš, 2002b, eqs. 60, 68). The crossvariances of theoretical travel times are set to zeros although they should be considered, because their calculation has not been coded yet.

Using the P–wave arrival times of Table 2, we determined the nonnormalized 3–D marginal a posteriori density functions (13) which describe the relative probability of the seismic hypocentres of the 4 events. The maxima of the nonnormalized 3–D marginal a posteriori density function and arrival–time misfit y defined by (22) resulting from the nonlinear hypocentre determination are displayed in Table 3.

<i>event</i>	$\sigma_{P_3}^{\max}$	y
1	0.569	1.126
2	0.686	0.754
3	0.605	1.007
4	0.908	0.193

Table 3: For each event, the maximum $\sigma_{P_3}^{\max}$ of the nonnormalized 3–D marginal a posteriori density function (13) which describes the relative probability of the seismic hypocentre, and arrival–time misfit y defined by (22).

The mean value of the arrival–time misfit should read (Bulant & Klimeš, 2015, eq. 48)

$$\langle y \rangle = N - 4 \quad , \quad (26)$$

where N is the number of measured arrival times. The average number of arrival times is $\bar{N} = 9$, see Table 2. The average arrival–time misfit

$$\bar{y} = 0.770 \quad (27)$$

in Table 3 is 6.5 times smaller than the average

$$\bar{N} - 4 = 5.000 \quad (28)$$

of the right–hand sides of estimation (26). This disagreement has probably two reasons:

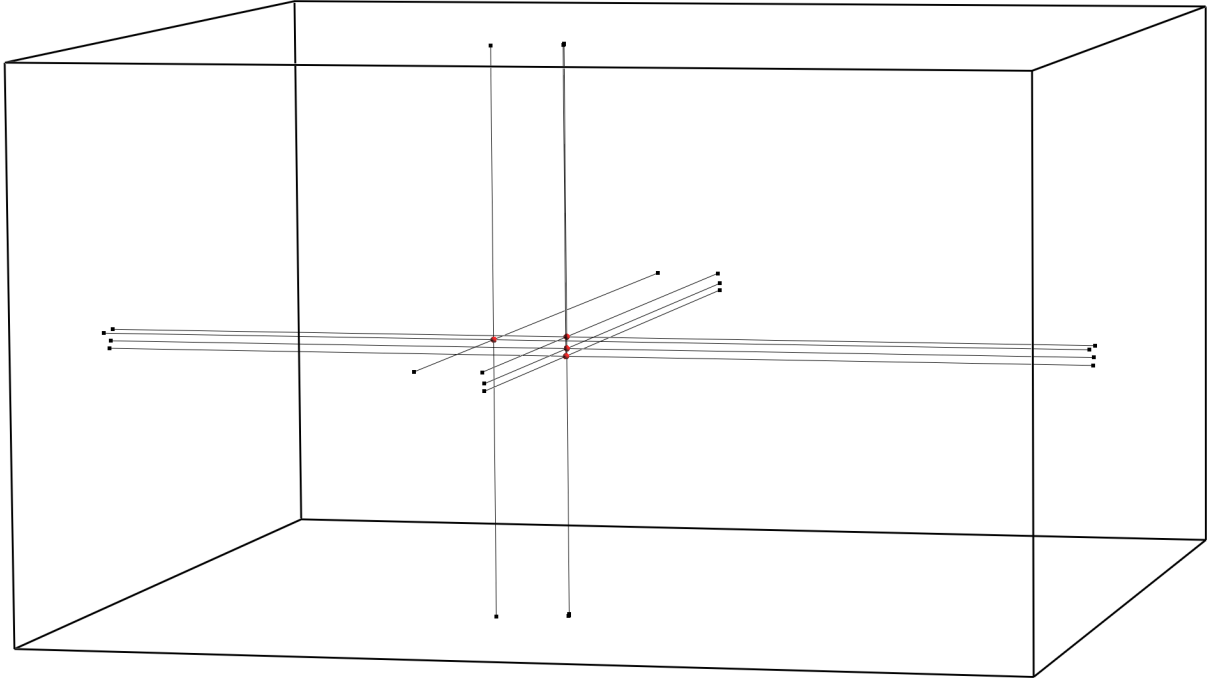


Figure 3: The locations of the centres of small cubes which are displayed as yardsticks in Figures 4–11 (small red spheres), together with their projections onto the sides of the grid used for the nonlinear hypocentre determination. The displayed dimensions of the grid used for the nonlinear hypocentre determination are $30 \text{ km} \times 30 \text{ km} \times 17 \text{ km}$.

1. Average arrival–time misfit $\bar{\gamma}$ resulting from our incorrect hypocentre determination with the zero crossvariances of theoretical travel times is smaller than the average of correct arrival–time misfits given by estimation (26), see Bulant & Klimeš (2015, sec. 6.3).
2. The 3–D Western Bohemia a priori velocity model may be more accurate than the 1–D mean model of the region by Klimeš (2002b, eq. 59), and standard deviations (1) of theoretical travel times with coefficients (23)–(25) may thus be overestimated.

Note that we may adjust overestimated factor σ in standard theoretical travel–time deviations (1) in such a way, that average arrival time misfit $\bar{\gamma}$ will correspond to its estimation $\bar{N}-4$, see the approach by Bulant & Klimeš (2015, sec. 7).

The nonnormalized marginal a posteriori density functions (13) describing the relative probability of the seismic hypocentres are displayed in Figures 4 to 7. The locations of the centres of small cubes which are displayed as yardsticks in Figures 4–11 are displayed in Figure 3. The details of these nonnormalized marginal a posteriori density functions are displayed in Figures 8 to 11. We can observe much greater uncertainty of the hypocentral position of event 4 determined just from six P–wave arrival times.

We have observed that the location of the maximum value of the nonnormalized 3–D marginal a posteriori density function may considerably differ from the mean hypocentre location given by the nonnormalized 3–D marginal a posteriori density function. Moreover, the mean hypocentre location often considerably depends on the dimensions of the location grid. Refer to Figure 7 for an obvious example.

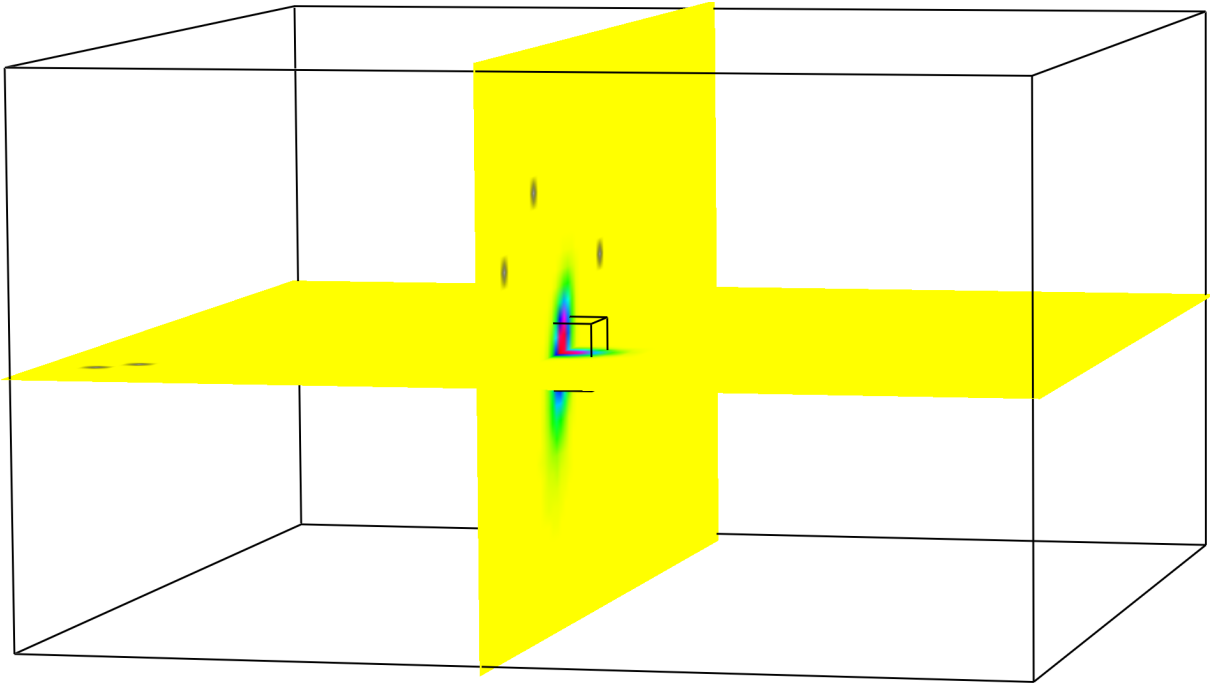


Figure 4: Nonnormalized 3-D marginal a posteriori density function of event 1 determined using 10 P-wave arrival times. The zero values are displayed in yellow. The nonzero values range through green, cyan, blue and magenta to the maximum value displayed in red. The undefined values are displayed in gray, and denote the gridpoints at which at least one theoretical travel time is missing. The small cube has the sides of 2 km.

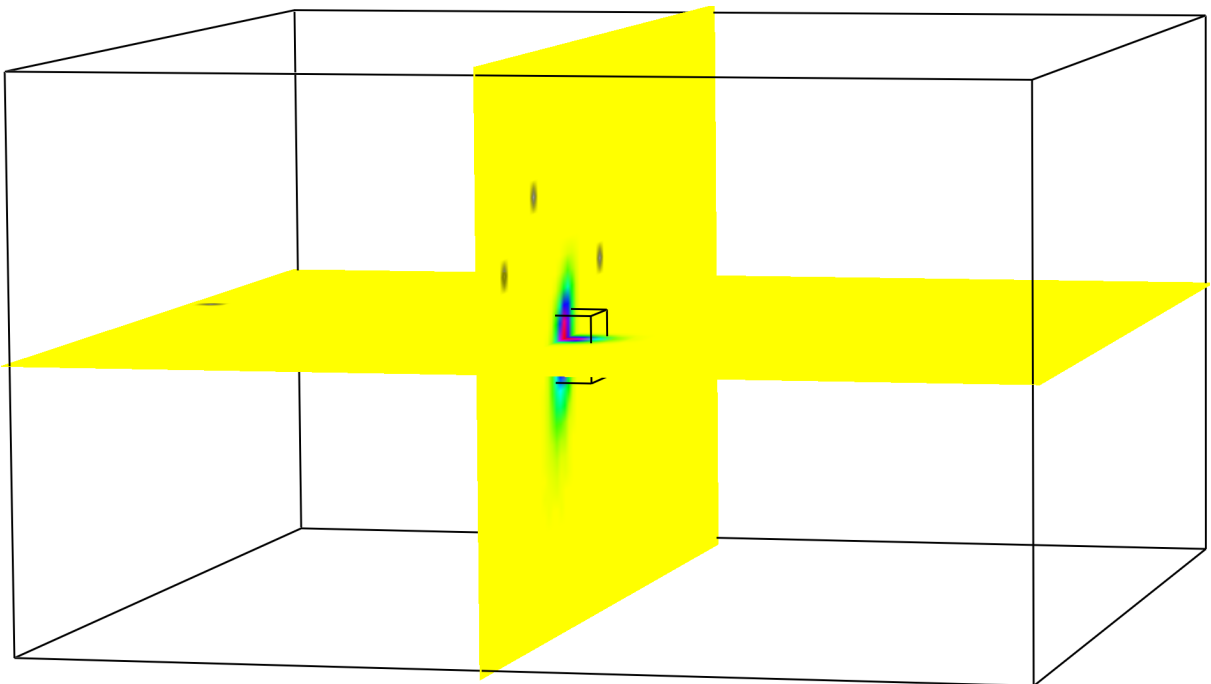


Figure 5: Nonnormalized 3-D marginal a posteriori density function of event 2 determined using 10 P-wave arrival times. The zero values are displayed in yellow. The nonzero values range through green, cyan, blue and magenta to the maximum value displayed in red. The undefined values are displayed in gray, and denote the gridpoints at which at least one theoretical travel time is missing. The small cube has the sides of 2 km.

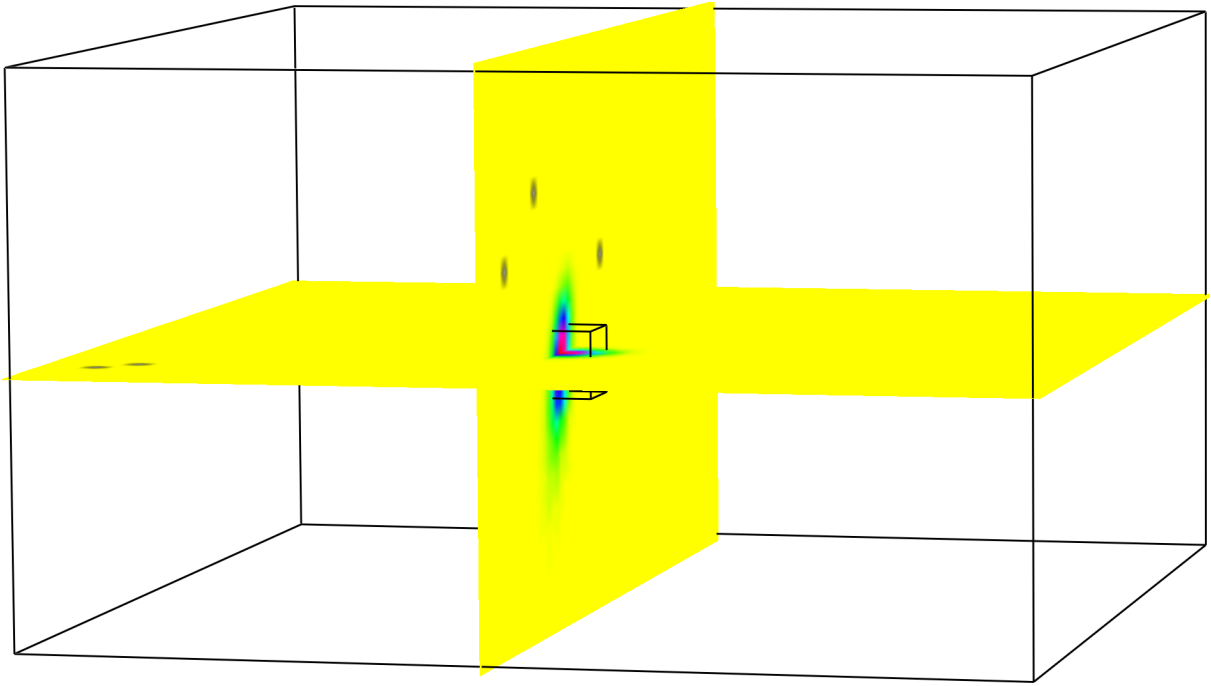


Figure 6: Nonnormalized 3-D marginal a posteriori density function of event 3 determined using 10 P-wave arrival times. The zero values are displayed in yellow. The nonzero values range through green, cyan, blue and magenta to the maximum value displayed in red. The undefined values are displayed in gray, and denote the gridpoints at which at least one theoretical travel time is missing. The small cube has the sides of 2 km.

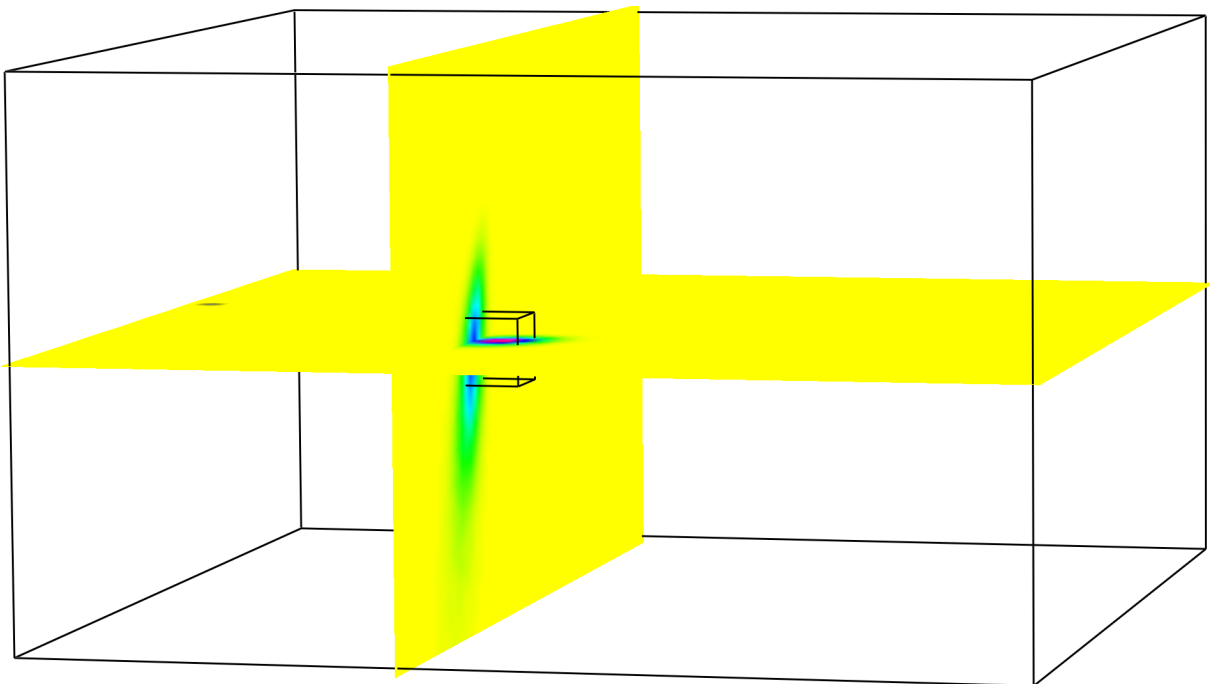


Figure 7: Nonnormalized 3-D marginal a posteriori density function of event 4 determined using 6 P-wave arrival times. The zero values are displayed in yellow. The nonzero values range through green, cyan, blue and magenta to the maximum value displayed in red. The undefined values are displayed in gray, and denote the gridpoints at which at least one theoretical travel time is missing. The small cube has the sides of 2 km.

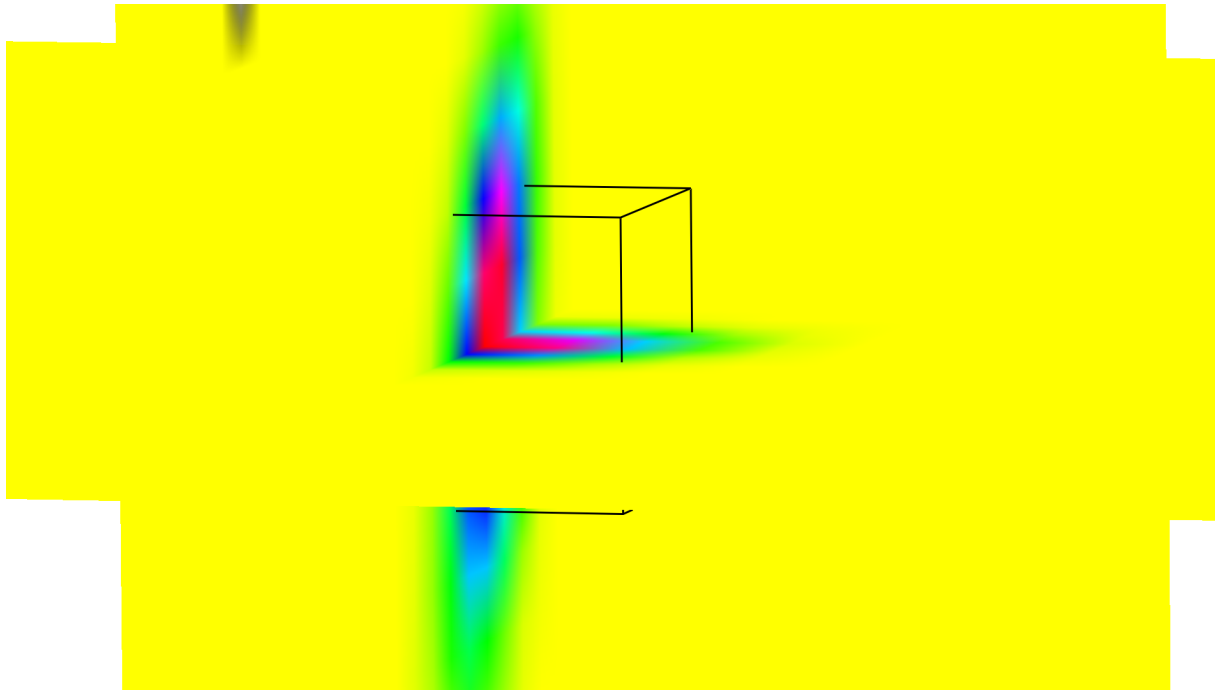


Figure 8: The detail of the interpolated discretized nonnormalized 3-D marginal a posteriori density function of event 1, displaying the hypocentral region of Figure 4. The cube has the sides of 2 km.

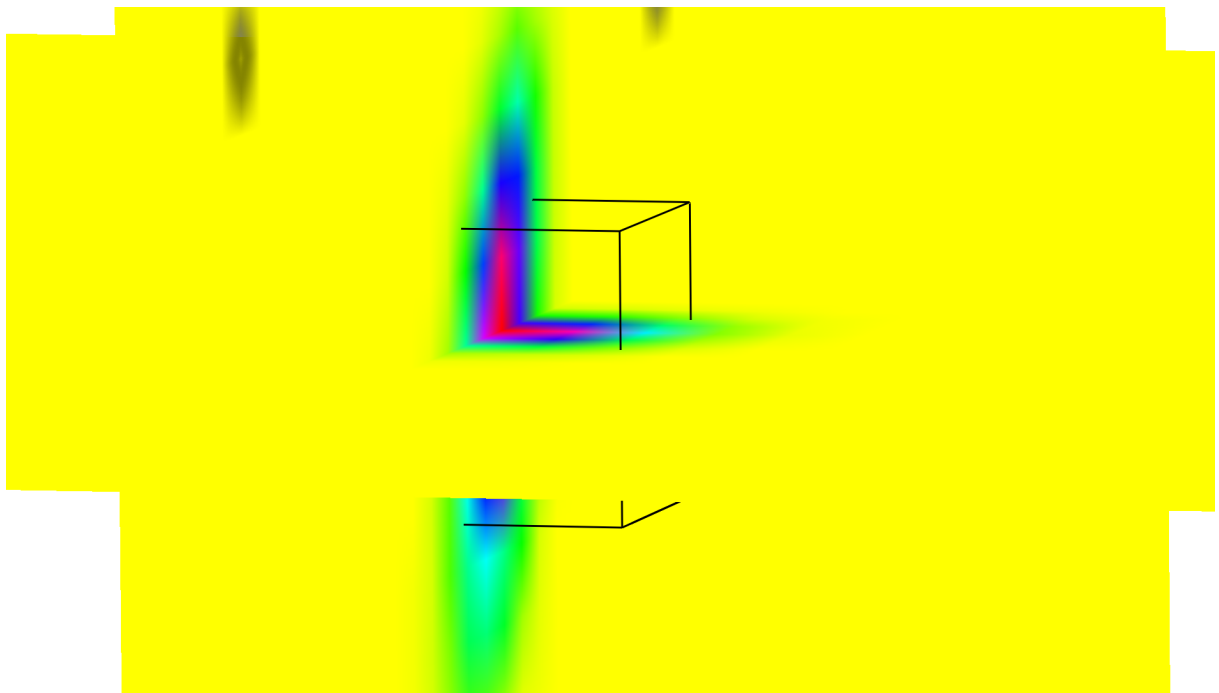


Figure 9: The detail of the interpolated discretized nonnormalized 3-D marginal a posteriori density function of event 2, displaying the hypocentral region of Figure 5. The cube has the sides of 2 km.

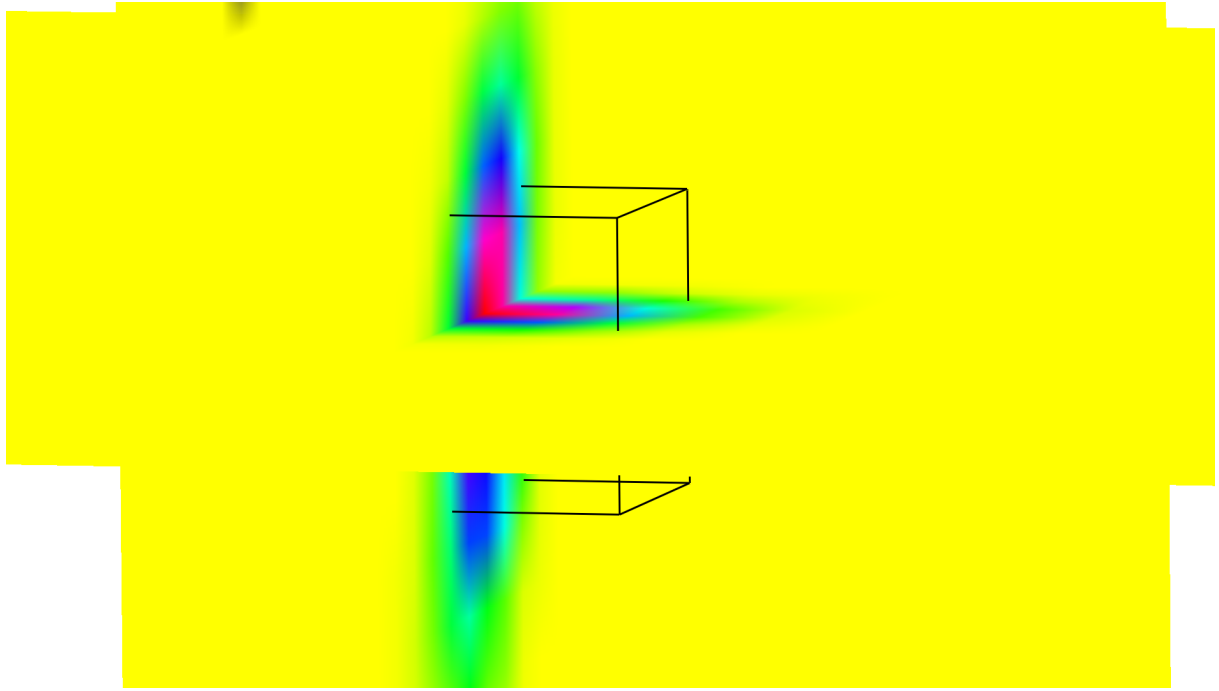


Figure 10: The detail of the interpolated discretized nonnormalized 3-D marginal a posteriori density function of event 3, displaying the hypocentral region of Figure 6. The cube has the sides of 2 km.

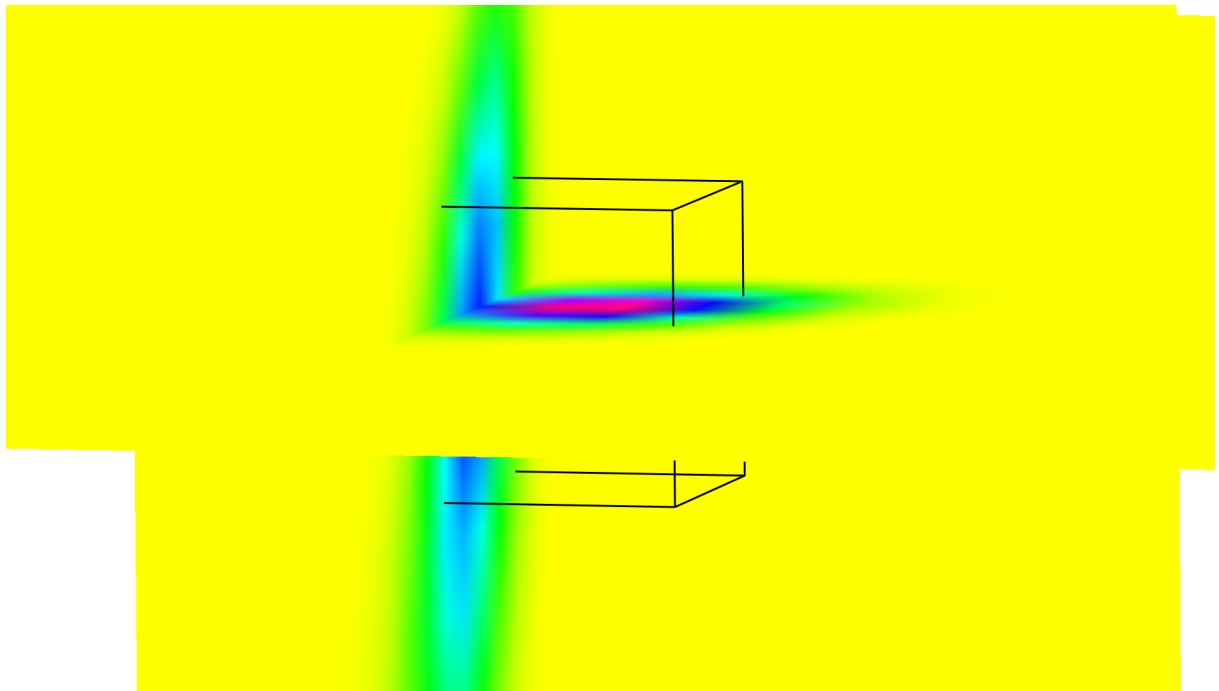


Figure 11: The detail of the interpolated discretized nonnormalized 3-D marginal a posteriori density function of event 4, displaying the hypocentral region of Figure 7. The cube has the sides of 2 km.

Acknowledgements

The research has been supported by the Grant Agency of the Czech Republic under contract P210/10/0736, by the Ministry of Education of the Czech Republic within research projects MSM0021620860 and CzechGeo/EPOS LM2010008, and by the members of the consortium “Seismic Waves in Complex 3-D Structures” (see “<http://sw3d.cz>”).

References

- Bucha, V. & Bulant, P. (eds.) (2015): SW3D-CD-19 (DVD-ROM). *Seismic Waves in Complex 3-D Structures*, **25**, 209–210, online at “<http://sw3d.cz>”.
- Bucha, V., Bulant, P. & Klimeš, L. (eds.) (2000): SW3D-CD-4 (CD-ROM). *Seismic Waves in Complex 3-D Structures*, **10**, 227–227, online at “<http://sw3d.cz>”.
- Bulant, P. (1996): Two-point ray tracing in 3-D. *Pure appl. Geophys.*, **148**, 421–447.
- Bulant, P. (1997): Calculation of multivalued ray-theory travel times at nodes of 3-D grids. *Seismic Waves in Complex 3-D Structures*, **6**, 71–74, online at “<http://sw3d.cz>”.
- Bulant, P. (1999): Two-point ray-tracing and controlled initial-value ray-tracing in 3-D heterogeneous block structures. *J. seism. Explor.*, **8**, 57–75, online at “<http://sw3d.cz>”.
- Bulant, P. (2012): Interpolation within ray tubes — state of the art. *Seismic Waves in Complex 3-D Structures*, **22**, 169–182, online at “<http://sw3d.cz>”.
- Bulant, P. & Klimeš, L. (1999): Interpolation of ray theory traveltimes within ray cells. *Geophys. J. int.*, **139**, 273–282, online at “<http://sw3d.cz>”.
- Bulant, P. & Klimeš, L. (2015): Nonlinear hypocentre determination. *Seismic Waves in Complex 3-D Structures*, **25**, 17–36, online at “<http://sw3d.cz>”.
- Červený, V., Klimeš, L. & Pšenčík, I. (1988): Complete seismic-ray tracing in three-dimensional structures. In: Doornbos, D.J. (ed.): *Seismological Algorithms*, pp. 89–168, Academic Press, New York.
- Franklin, J.N. (1970): Well-posed stochastic extensions of ill-posed linear problems. *J. math. Anal. Appl.*, **31**, 682–716.
- Klimeš, L. (ed.) (1998): SW3D-CD-2 (CD-ROM). *Seismic Waves in Complex 3-D Structures*, **7**, 405–405, online at “<http://sw3d.cz/software/sw3dcd2/index.htm>”.
- Klimeš, L. (1995): Examples of seismic models. *Seismic Waves in Complex 3-D Structures*, **3**, 5–35, online at “<http://sw3d.cz>”.
- Klimeš, L. (2002a): Application of the medium covariance functions to travel-time tomography. *Pure appl. Geophys.*, **159**, 1791–1810, online at “<http://sw3d.cz>”.
- Klimeš, L. (2002b): Estimating the correlation function of a self-affine random medium. *Pure appl. Geophys.*, **159**, 1833–1853, online at “<http://sw3d.cz>”.
- Moser, T-J., Van Eck, T. & Nolet, G. (1992): Hypocenter determination in strongly heterogeneous Earth models using the shortest path method. *Journal of Geophysical Research*, **97B**, 6563–6572.
- Tarantola, A. (1987): *Inverse Problem Theory*. Elsevier, Amsterdam.
- Tarantola, A. & Nercessian, A. (1984): Three-dimensional inversion without blocks. *Geophys. J. Roy. astr. Soc.*, **76**, 299–306.
- Tarantola, A. & Valette, B. (1982): Inverse problems = quest for information. *J. Geophys.*, **50**, 159–170.